RSC Advances

PAPER

View Article Online
View Journal | View Issue

Cite this: *RSC Adv.*, 2017, **7**, 7358

Silver(I) coordination polymers with 3,3′,5,5′-tetrasubstituted 4,4′-bipyridine ligands: towards new porous chiral materials†

E. Aubert,*[a] M. Abboud,[ab] A. Doudouh,[a] P. Durand,[a] P. Peluso,[c] A. Ligresti,[d] B. Vigolo,[e] S. Cossu,[f] P. Pale[g] and V. Mamane*[g]

Received 14th December 2016
Accepted 13th January 2017

DOI: 10.1039/c6ra28197d

www.rsc.org/advances

Coordination polymers (CP) assembled from 3,3′,5,5′-tetrasubstituted 4,4′-bipyridines and silver salts have been prepared and characterized by X-ray diffraction. Silver-CPs based on infinite Ag–bipyridine chains were obtained where one or two halogen atoms strongly interacted with Ag. A homochiral MOF was also prepared using the enantiopure 3,3′-dibromo-5,5′-bis(4-methoxyphenyl)-4,4′-bipyridine as ligand, while its racemic form only formed a compact CP. Preliminary applications showed that the homochiral network is able to recognize the enantiomers of *rac*-styrene oxide and to control the cytotoxicity level of the Ag-based MOF toward a cell line derived from adult human skin (HaCaT).

Introduction

Metal–organic frameworks (MOFs) are tri-dimensional coordination polymers (CPs) in which permanent porosity is present.[1] These architectures are conveniently obtained by directional association of metal ions and polytopic ligands. With the right selection of metal coordination sphere and ligand, different framework and cavity shapes and sizes could be obtained and tuned for various applications.[2] Among the latter, gas storage[3] and separation[4] are the most advanced, but catalysis[5] and biomedical applications[6] are gaining more and more interest.

MOFs can be made homochiral by using homochiral ligands to build them. Such homochiral MOFs could be exploited for enantioselective organic transformations[7] and separations.[8] So far, chiral ligands derived from the natural chiral pool have mostly been employed,[9] but synthetic chiral ligands, such as salen,[10] biphenyl and binaphtyl derivatives,[11] have been also reported. Although 4,4′-bipyridine was extensively used as ditopic ligand in CPs,[12] only one example of homochiral MOF containing a 4,4′-bipyridine motif has so far been reported.[13] In this case, the rigid ditopic linker contains a chiral substituent which provides the chiral information. As already mentioned, axial chirality has been exploited for the synthesis of chiral linkers. Nevertheless, to date no atropisomeric 4,4′-bipyridine has been used for the construction of homochiral MOF. In this regard, it is worth mentioning that atropisomeric ligands derived from tetramethylated 4,4′-bipyridines have been used to build metallo-supramolecular squares.[14]

In the last few years, our group described new protocols for the preparation[15] and enantioseparation[16] of chiral polyhalogenated 4,4′-bipyridines, which appear to be versatile chiral linkers for the preparation of new homochiral MOFs. Indeed, the presence of halogen groups in these 4,4′-bipyridines should be highly beneficial. Besides inducing atropoisomerism by restricted rotation around the 4,4′-axis, they should allow to tune the cavity shape and size of the corresponding MOFs through either halogen change or functionalization by palladium cross-coupling reactions. Furthermore, they should induce various interactions with molecules, allowing enantioselective discrimination and thus separation. In particular, recently, we found that polyhalogenated 4,4′-bipyridines can serve as halogen bond donors both in solution[16c,e] and in the solid state.[15a,d]

In the present report, we describe the synthesis and X-ray structure of CPs and MOFs based on silver(I) and tetrasubstituted 4,4′-bipyridines **L1–L5** (Scheme 1). Moreover, with the aim to investigate both recognition capability and bioactivity of the homochiral network based on **L5**, the findings of some preliminary applications are described herein. Silver(I) was selected as connecting metal for the following reasons: (a) CPs

[a]*Cristallographie, Résonance Magnétique et Modélisations (CRM2). UMR CNRS 7036, Université de Lorraine, BP 70239, Bd des Aiguillettes, Vandoeuvre-les-Nancy 54506, France. E-mail: emmanuel.aubert@univ-lorraine.fr*

[b]*Laboratoire SRSMC, UMR CNRS 7565, Université de Lorraine, BP 70239, Bd des Aiguillettes, Vandoeuvre-les-Nancy 54506, France*

[c]*Istituto di Chimica Biomolecolare ICB CNR – Sede secondaria di Sassari, Traversa La Crucca 3, Regione Baldinca, I-07100 Li Punti – Sassari, Italy*

[d]*Istituto di Chimica Biomolecolare ICB CNR – Via Campi Flegrei 34, I-80078 Pozzuoli (Na), Italy*

[e]*Institut Jean Lamour, CNRS-Université de Lorraine, BP 70239 Bd des Aiguillettes, Vandœuvre-lès-Nancy 54506, France*

[f]*Dipartimento di Scienze Molecolari e Nanosistemi, Università Ca' Foscari di Venezia, Via Torino 155, I-30172 Mestre Venezia, Italy*

[g]*Institut de Chimie de Strasbourg, UMR 7177, Equipe LASYROC, 1 rue Blaise Pascal, BP 296 R8, Strasbourg Cedex 67008, France. E-mail: vmamane@unistra.fr*

† Electronic supplementary information (ESI) available. CCDC 1439676–1439686. For ESI and crystallographic data in CIF or other electronic format see DOI: 10.1039/c6ra28197d

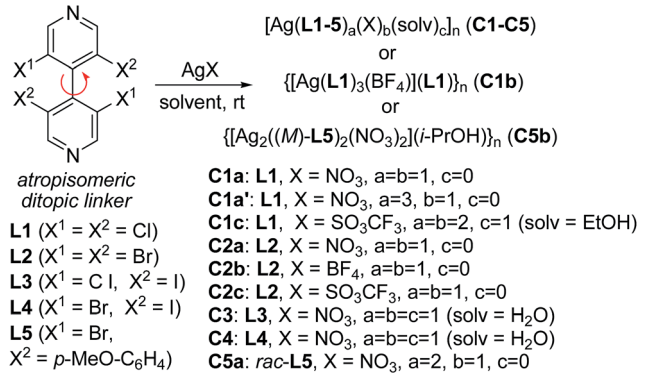

Scheme 1 Synthesis of Ag(I)-CPs from achiral and chiral 4,4′-bipyridines.

based on Ag(I) often lead to crystalline solids, allowing investigation by single-crystal X-ray diffraction;[17] (b) Ag(I) can adopt coordination numbers between two and six, and thus various geometries; (c) Ag(I) coordination is known to be affected by weak intermolecular forces, such as argentophilic[18] and halophilic interactions;[19] (d) silver is a well-known antibacterial agent[20] and its antimicrobial properties have been extensively exploited in silver-exchanged zeolites technology.[21] In this context, the designed silver/bipyridine-based MOFs could be envisaged as bioactive coordination networks.

Experimental section

General

All chemicals and reagents were used as received from the supplier. Ligands **L1–L5** were prepared according to our procedures.[15a,b] Elemental analyses were carried out with the ThermoFisher Scientific Flash 2000 CHNS elemental analyser at the Institute of Chemistry, University of Strasbourg, France. The FT-IR spectra were recorded on a Nicolet 5700 FT-IR Thermo Scientific spectrophotometer in the range of 400–4000 cm^{-1}. The sample was mixed with KBr and pellet technique was used to record the spectrum.

X-ray crystallography

Low-temperature (110 K) X-ray diffraction experiments were performed with an Oxford XCalibur diffractometer operating with Mo-K_α or Cu-K_α radiations. The data collections and reductions were performed using the CrysAlisPro software [CrysAlisPro, Oxford Diffraction Ltd. 2009–2012]. Absorption corrections were performed analytically using multifaceted crystal models.[22] Structure solutions and refinements were performed within WinGX software[23] with programs SIR92 and SHELXL-97.[24] Figures were made with the help of Mercury.[25]

CCDC 1439676–1439686 contain the supplementary crystallographic data.

Theoretical calculations

Density functional theory calculations on CP **C1a** were performed using the Gaussian09 program package.[26] The ωB97XD functional was used together with the cc-pVTZ basis set, the latter being completed with a pseudo-potential for silver atoms. Topological analyses of the electron density were performed using the AIMAll software.[27] Periodic DFT calculations were performed on CP **C4** within Castep software[28] using plane wave basis and built-in ultrasoft pseudopotentials. The PBE functional was used,[29] as completed with the semiempirical dispersion correction of Grimme.[30]

HPLC

An Agilent Technologies (Waldbronn, Germany) 1100 Series HPLC system (high-pressure binary gradient system equipped with a diode-array detector operating at multiple wave-lengths, a programmable autosampler with a 20 μL loop, and a thermostatted column compartment) was employed. Data acquisition and analyses were carried out with Agilent Technologies ChemStation Version B.04.03 chromatographic data software. The UV absorbance is reported as milliabsorbance units (mAU). Lux Cellulose-2 (Phenomenex, USA) (cellulose tris-3-chloro-4-methylphenylcarbamate; 5 μm) was used as chiral column (250 × 4.6 mm). HPLC grade *n*-hexane and 2-propanol were purchased from Sigma-Aldrich (Taufkirchen, Germany). Analyses were performed in isocratic mode at 22 °C. The flow rate (FR) was set at 0.8 mL min^{-1}. The enantiomer elution order (EEO) was determined by injecting enantiomers of known absolute configuration.

Cytotoxicity assay

Immortalized HaCaT cells were purchased from ATCC (Manassas, VA, USA) and routinely grown in Dulbecco's modified Eagle's medium (DMEM) supplemented with 2 mM L-glutamine, 100 U mL^{-1} penicillin/100 L g mL^{-1} streptomycin and 10% fetal bovine serum (FBS). Cells were seeded in a 24-well plate at 3×10^4 cell per well, and cultured overnight at 37 °C in a 5% CO_2 atmosphere. Test compounds were incubated for different time points (24–48–72 h). Following incubation, media were replaced with a MTT solution (0.5 mg mL^{-1}) and cultured for additional 3 hours. Formazan (MTT metabolic product) was resuspended by isopropanol and absorbance at 620 nm was read on a GENios-Pro 96/384 Multifunction Microplate Reader. Optical density values from vehicle-treated cells were considered as 100% of cell viability and the results were expressed as a percentage (%) of the control (vehicle alone). Data are given as the mean from five independent experiments conducted in triplicate.

General procedures for the synthesis of silver CPs

Method A. A mixture of $AgNO_3$ (8.5 mg, 0.05 mmol), **L** (0.05 mmol), H_2O (1 mL), i-PrOH (2 mL) and CH_3CN (1 mL) was stirred in the absence of light for 10 min to give a clear solution. The mixture was allowed to stand at room temperature with slow evaporation of the solvents. After 5 days, colorless crystals suitable for X-ray diffraction were collected, washed with water, ether and dried at room temperature under vacuum.

This method was used for the preparation of complexes **C1a** (45%), **C1a′** (53%; MeOH was used instead of i-PrOH), **C2a** (42%), **C3** (58%), **C4** (60%), **C5a** (70%) and **C5b** (53%).

Method B. To a solution of AgX (X = BF_4 or TfO, 0.03 mmol) in ethanol (2 mL) was added a solution of **L1** or **L2** (0.03 mmol) in chloroform (0.5 mL). The mixture was stirred for 15 min then allowed to stand at room temperature with slow evaporation of the solvents. After 5 days, colorless crystals suitable for X-ray diffraction were collected, washed with ethanol and dried at room temperature under vacuum. This method was used for the preparation of complexes **C1b** (35%), **C1c** (39%), **C2b** (48%) and **C2c** (37%).

All the prepared CPs are insoluble in water and most of organic solvents. They are slightly soluble in alcoholic solvents (ethanol, isopropanol and methanol).

Results and discussion

CPs based on 4,4′-bipyridine often lead to 1D polymer with linear geometry, but depending on the anion, more complex geometries such as zigzag-chain or grid in 2-3D frameworks could be obtained.[12] As ladder and grid structures offer open space, it is worth to look for such arrangements for building MOFs. As such structures are more frequent when the anions are nitrates,[12a] we privileged such anions with our polyhalogeno-4,4′-bipyridines. Nevertheless, in order to explore the coordination and geometries with these novel ligands, we screened various silver salts with anions of different geometry and coordination ability (Scheme 1).

Ag(I) CPs of achiral bipyridines L1 and L2: anion effect

The achiral 4,4′-bipyridines **L1** and **L2** were considered first as model ligands to probe the formation of MOFs. They were thus submitted to various silver salts in various conditions. In the absence of light, most combinations readily evolved to clear solutions within 10–15 min. Upon standing under various crystallization conditions, crystals were obtained for some combinations. Determined by single crystal X-ray diffraction (XRD; see Table S1, ESI†), their structures proved unexpectedly diverse, with interesting features described below.

Despite their homology and relative simplicity, the tetrachloro- or bromobipyridines **L1** and **L2** form very different architectures, depending on the silver counter-ion. With silver nitrate, bipyridines **L1** and **L2** produced in high yields colorless CPs **C1a** and **C2a** respectively, of formulas [Ag(**L1** or **L2**)$(NO_3)]_n$. Both crystallize in the monoclinic $P2_1$ space group and are isostructural, although the unit cell volume of the latter was larger due to the larger radius of bromine atom compared to chlorine. The XRD structure revealed that these CPs are composed of zigzag bipyridine–silver chains (N–Ag–N = 146.5° and 142.30°, respectively) along [201] direction (Fig. 1). Interestingly, the silver coordination proved more complex, connecting adjacent zigzag chains and allowing the formation of non-interpenetrating 3D network. Indeed, beside the two nitrogen atoms of two bipyridines, three oxygen atoms belonging to two nitrate anions coordinate the metal center in

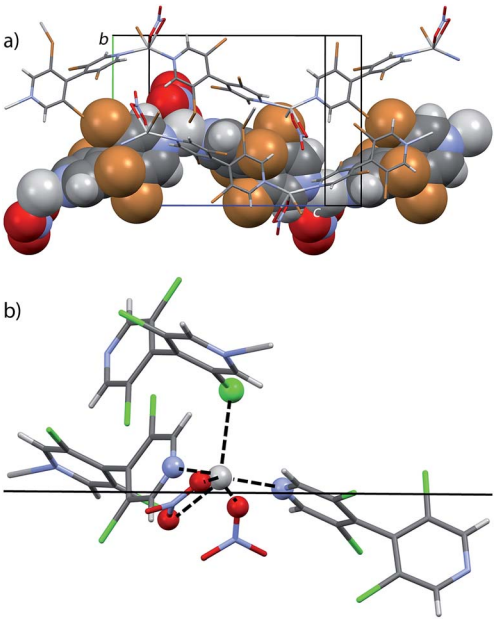

Fig. 1 (a) XRD structure of silver 3,3′,5,5′-tetrabromo-4,4′-bipyridine nitrate CP **C2a**, revealing the zigzag arrangement of such CPs. Brown, blue, red, dark and light gray, silver represent Br, N, O, C, H, Ag respectively. (b) Coordination around Ag(I) in the silver 3,3′,5,5′-tetrachloro-4,4′-bipyridine nitrate CP **C1a**. The trace of the mean plane defined by N (blue) and O (red) atoms is depicted as the black horizontal line. The chlorine atom showing a type-II halogen bond with silver is shown as green sphere.

a roughly planar disposition, the distance from the Ag atom to the O, N mean plane being 0.525 Å and 0.575 Å, respectively (Fig. 1b). The coordination sphere of the metal ion is further completed by one halogen atom of a bipyridine belonging to an adjacent chain. The halogen to silver distances (Ag···Cl = 3.043 Å, Ag···Cl–C = 115.96°; Ag···Br = 3.134 Å, Ag···Br–C = 114.38°) are shorter than the sum of the corresponding van der Waals radii, (r_{vdW}(Ag) + r_{vdW}(Cl) = 3.47 Å and r_{vdW} (Ag) + r_{vdW}(Br) = 3.57 Å),[31] as already reported in the literature,[19] suggesting bonding between these atoms. This halogen seems to interact with silver through its negatively charged crown according to the sigma hole model, as in type-II halogen bonds.[32] To get more insights into these interactions, quantum chemistry calculations were performed at the density functional level of theory on CP **C1a**. The AIM topological analysis of the computed electron density revealed a bond critical point between the metal and the halogen atoms (see Fig. S1, ESI†), where the electron density (ρ_{CP} = 0.018 a.u.) and its positive Laplacian ($\nabla^2\rho_{CP}$ = +0.061 a.u.) indicate the close-shell nature of this interaction. By comparison, this electron density is in between the values displayed at the critical points associated to the long (3.107 Å, ρ_{CP} = 0.010 a.u.) and short (2.523 Å, ρ_{CP} = 0.034 a.u.) Ag···O bonds, underlying the relative importance of that particular interaction for the coordination around the metal center; moreover, the electron density obtained at the Ag···Cl bond in **C1a** is larger than the values found in Cl···Cl type II halogen bonds implying neutral molecules (ρ_{CP} = 0.006 a.u.).[33]

These coordinations through nitrate ions and one bipyridine halogen strongly bond together the bipyridine–silver chains. The strongest interactions arise through the nitrate anions, which form planes parallel to (10−2), orthogonal to the bipyridine–silver chain mean plane. Furthermore, these planes interact through the previously described Ag···Cl, Br interaction and another halogen bond formed with one oxygen atom of the nitrate anion, where the electrophilic sigma hole of the halogen points toward the negative charge of the anion (O···Cl = 3.040 Å, O···Cl–C = 169.93°; O···Br = 3.083 Å, O···Br–C = 171.00°) (see Fig. S2, ESI†).

In the case of bipyridine **L1**, a second structure was surprisingly observed. XRD revealed a different topology with the formula $[Ag(\mathbf{L1})_3(NO_3)]_n$. In this CP **C1a′**, silver exhibits trigonal bipyramidal coordination with three bipyridine ligands as the triangular base and two nitrate oxygen atoms at the apical positions (Fig. 2). Thus, infinite Ag···NO_3 chains are formed along [010] which interact through numerous C–H···O, N and Cl···Cl contacts. Contrarily to the previous $[Ag(\mathbf{L1})(NO_3)]_n$ CP **C1a**, no halogen–metal interaction is present in this structure.

Changing the counter anion to BF_4^- leads to different results depending on the ligand. For bipyridine **L2**, the formed CP $[Ag(\mathbf{L2})(BF_4)]_n$ (**C2b**) is isostructural to the one obtained with NO_3^- (**C2a**), although the bipyridine–silver chains are closer to linearity (N–Ag–N = 170.35° *vs.* 142.30°) and the anion-metal distance is much larger (3.433 Å *vs.* 2.926 Å) (Fig. 3a). This flattening seems to weaken the inter-chain halogen···silver interaction, as shown by the elongated bond distance (Ag···Br = 3.474 Å *vs.* Ag···Br = 3.134 Å).

With bipyridine **L1**, new crystals from the *P*2/*c* space group were obtained with the formula $\{[Ag(\mathbf{L1})_3(BF_4)](\mathbf{L1})\}_n$ **C1b** (Fig. 3b). In this new CP, silver ion is coordinated by four bipyridines and two anions (Ag···B = 3.299 Å, 4.295 Å). Two of these bipyridines coordinate silver from both nitrogen atoms, leading to bipyridine···silver chains parallel to [100]. These chains are bonded together through the anions, forming planes parallel to (001), which are held together by aromatic C–H···N hydrogen bonds (H···N = 2.57 Å). Such arrangement leads to a MOF 3D network displaying channels along [010] (free diameter 3.5 Å × 6.5 Å), crossing smaller channels parallel to [100] (free diameter 2.8 Å × 6.0 Å). This MOF structure offers thus a rather large open volume (1316 Å^3 *i.e.* 42% of the unit cell volume, see Fig. S3, ESI†), which could be used for the trapping

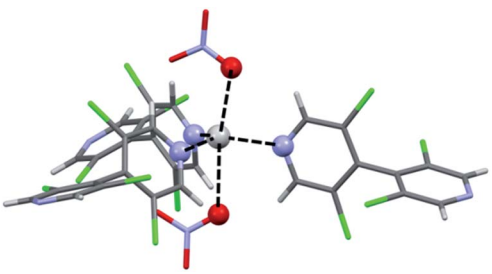

Fig. 2 Coordination around Ag(I) in the silver 3,3′,5,5′-tetrachloro-4,4′-bipyridine nitrate CP **C1a′**. Bond distances are: Ag···N = 2.290 Å, 2.318 Å, 2.307 Å; Ag···O = 2.551 Å, 2.764 Å.

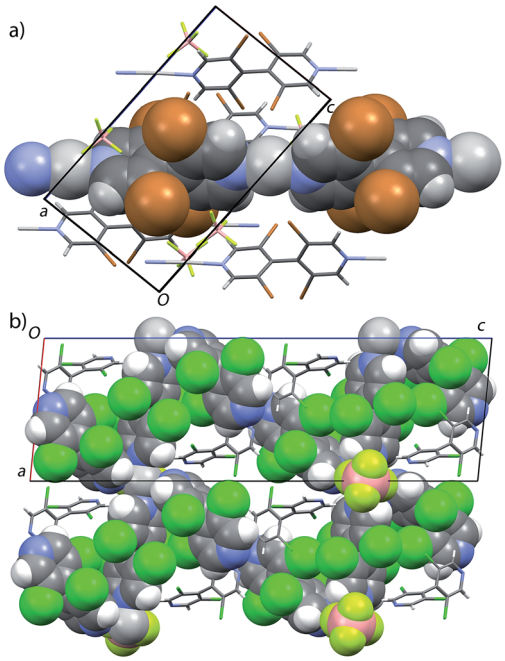

Fig. 3 (a) XRD structure of silver 3,3′,5,5′-tetrabromo-4,4′-bipyridine tetrafluoroborate CP **C2b**, revealing the almost linear arrangement of this CP. (b) View along [010] in the silver 3,3′,5,5′-tetrachloro-4,4′-bipyridine tetrafluoroborate CP **C1b**. The molecules belonging to the coordination network are displayed as sphere using van der Waals radii, whereas uncoordinated bipyridine molecules occupying the so-formed channels are shown as sticks. Color coding as above.

or separation of compounds. Interestingly, the voids of the so-formed MOF are already occupied by uncoordinated bipyridine molecules in the larger channel.

Using silver triflate to build up CPs with the tetrachloro- or bromobipyridines **L1** or **L2** led again to other and new structures. With **L2**, orthorhombic crystals from the *Cmca* space group with formula $[Ag(\mathbf{L2})(SO_3CF_3)]_n$ were obtained. The same 1D bipyridine···silver chain than in other **L2** CPs with $AgNO_3$ **C2a** and $AgBF_4$ **C2b** is again responsible for the main structure of this CP **C2c**. Interestingly, these chains more and more tend towards linearity depending on the counterion nature (N–Ag–N = 177.93° *vs.* 170.35° *vs.* 142.30, for respectively triflate, tetrafluoroborate and nitrate anion). In this case, the triflate anion contributes twice to the silver coordination in an almost square planar arrangement, with the distance from the Ag atom to the O, N mean plane being 0.462 Å (Fig. 4a).

As in the $[Ag(\mathbf{L1}\text{ or }\mathbf{L2})(NO_3)]_n$ CPs **C1a** or **C2a**, silver–halogen bonds further complete the metal coordination sphere, but instead of one interaction, two bromine···silver halogen bonds provided by the same bipyridine are present (Ag···Br = 3.320 Å, Ag···Br–C = 103.22°) as shown in Fig. 4b. Such bonding interactions connect the bipyridine–Ag chains together in a compact structure.

Bipyridine **L1** may form similar structure but crystals of suitable quality could not be obtained with $AgSO_3CF_3$. In order to solve this problem, recrystallization was attempted by adding ethanol to the solution. Under these conditions, triclinic

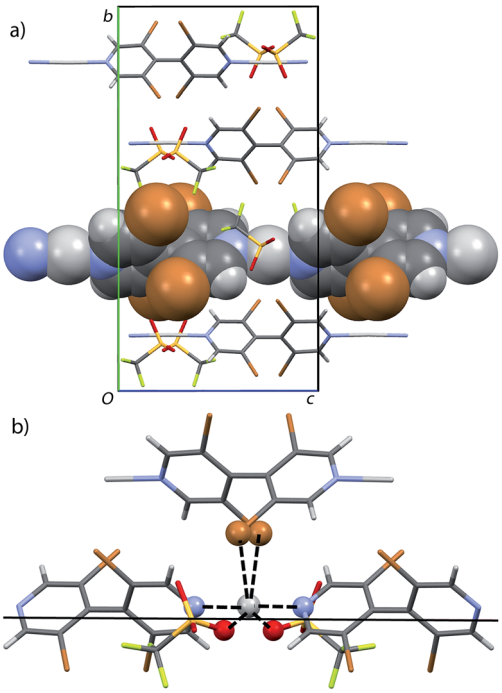

Fig. 4 (a) XRD structure of silver 3,3′,5,5′-tetrabromo-4,4′-bipyridine triflate CP **C2c**, revealing the linear and parallel arrangement of this CP. (b) Coordination around Ag(I) **C2c**. The trace of the mean plane defined by N (blue) and O (red) atoms is depicted as the black horizontal line. The bromine atoms showing a type-II halogen bond with silver are shown as brown spheres. Color coding as above.

crystals were produced from the $P\bar{1}$ space group. Their structure **C1c** showed that the cosolvent has become a constituent, with the formula $[Ag_2(\mathbf{L1})_2(SO_3CF_3)_2(EtOH)]_n$, and that two crystallographically independent silver atoms are present with different coordination spheres. Although both are coordinated by two bipyridine molecules, the main difference arises from the interactions with oxygen atoms. Around one of these silver cations, the coordination is completed with one oxygen atom of two triflate anions (Ag···O = 2.528 Å, 2.583 Å), as in the parent CP $[Ag(\mathbf{L2})(SO_3CF_3)]_n$ **C2c**. The other silver cation is surrounded by two oxygen atoms of the same triflate anion (Ag···O = 2.571 Å, 3.019 Å) but also is interacting with the oxygen atom of the ethanol molecule (Ag···O = 2.595 Å). Overall, this arrangement produces again 1D bipyridine···silver chains, in which the two types of Ag coordination alternate. Contrarily to what is obtained with bipyridine **L2**, no halogen–silver interaction is found; the chains interact through the triflate anions and also through hydrogen bonding between EtOH and triflate anions (O···O = 2.795 Å) which coordinate silver (Fig. 5).

These results showed, as expected, that CPs of bipyridines **L1** and **L2** could be achieved with Ag(I) salts. Interestingly, the brominated bipyridine **L2** always gave the same structure whatever the Ag anion, with the expected linear Ag–bipyridine chains interconnected by Ag-anion chains in roughly 2D plane, each being connected to the next plane by Ag–halogen bond (see Fig. 1a, 3a and 4). Unfortunately, such networks do not leave enough space for producing a MOF. In contrast, the less bulky

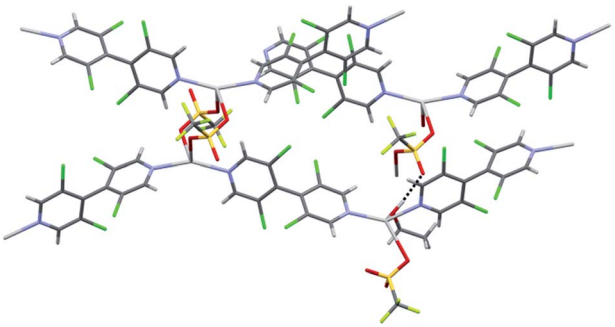

Fig. 5 XRD structure of silver 3,3′,5,5′-tetrachloro-4,4′-bipyridine triflate CP **C1c**. Color coding as above. Three chains interacting through the triflate anions and one EtOH molecule are displayed (hydrogen bond shown as dashed line).

and less electron-rich chlorinated bipyridine **L1** does not form the same network, except for one structure obtained with $AgNO_3$ (see Fig. 1b). Each anion induces a unique but different organization, from trigonal bipyramidal to octahedral coordination around silver ions. Rewardingly, a MOF with 42% open space was produced by using BF_4 as anion.

Crystal structures of Ag(I) CPs of chiral bipyridines L3 and L4

In a next series of experiments, CPs of chiral bipyridines **L3** and **L4** with $AgNO_3$ were prepared by using the previously established procedures. Both chiral but racemic tetrahalogenated bipyridine **L3** and **L4** provided crystals and their structures were determined by single crystal X-ray diffraction (Table S2, ESI†).

Both CPs exhibit inclusion of one water molecule per asymmetric unit ($[Ag(\mathbf{L3})(NO_3)(H_2O)]_n$ **C3** and $[Ag(\mathbf{L4})(NO_3)(H_2O)]_n$ **C4**) and present some orientational/configurational disorder affecting the halogen atomic positions. As in the preceding CPs, linear bipyridine···silver chains are observed in both **C3** and **C4** CPs, but the Ag(I) coordination is slightly different in each. In **C3**, the linear bipyridine···silver chains are almost homochiral (with a slight disorder of about 10%) whereas the high degree of disorder in **C4** preclude any statement about the enantiomer alternation along the chains in that coordination polymer.

In the chloro CP **C3**, a water molecule (Ag···O = 2.761 Å) and two nitrate anions participate in the coordination through three oxygen atoms (Ag···O = 2.838 Å, 2.856 Å, 3.018 Å), as well as two iodine atoms (Ag···I = 3.418 Å, 3.692 Å) (Fig. 6).

In the bromo CP **C4**, one oxygen atom of a nitrate anion (Ag···O = 2.660 Å), one oxygen atom of a water molecule (Ag···O = 2.474 Å) and two iodine atoms of an adjacent bipyridine (Ag···I = 3.210 Å, 3.235 Å) form the basal plane of a distorted square bipyramid (Fig. 7). Remarkably, in the crystal structure of CP **C4**, only the bromine and iodine atoms belonging to the same pyridine ring are subject to disorder, while the second half of the bipyridine remains perfectly ordered. Interestingly, this disorder affects the position *trans* to the water molecule, but not the position *trans* to the nitrate anion. As the refinement of the structure in a lower symmetry space group was not conclusive (*i.e.* disorder was still present),

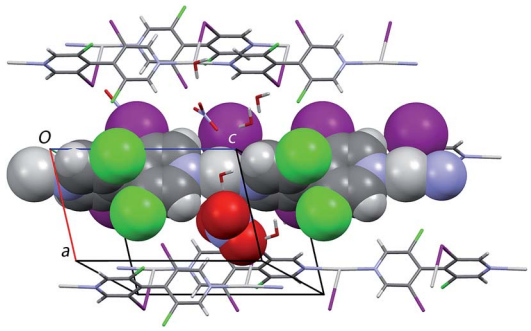

Fig. 6 Coordination around Ag(I) in silver 3,5-dichloro-3′,5′-diiodo-4,4′-bipyridine nitrate CP **C3**.

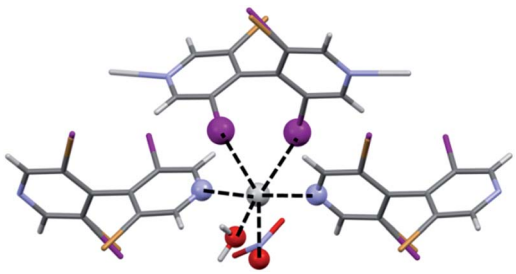

Fig. 7 Coordination around Ag(I) in the silver 3,5-dibromo-3′,5′-diiodo-4,4′-bipyridine nitrate CP **C4**. The two iodine atoms showing a type-II halogen bond with silver, being in *trans* position with respect to the water molecule and the nitrate anion, are shown as violet spheres. Disorders at half the halogen atoms are visualized on the figure.

we performed periodic DFT calculations assuming different coordination modes around the metal center with different set of halogen atoms located in *trans* position with respect to water/nitrate coordinating groups respectively (*e.g.* (i) I/I; (ii) I/Br; (iii) Br/I and (iv) Br/Br (see Fig. S4, ESI†)). In such a way, four different crystal phases were considered, and their atomic positions optimized at that level of theory. The lowest energy structure was found with two iodine atoms interacting with the metal center (i) (Ag···I = 3.393 Å and 3.091 Å); the second lowest energy structure, which is only 1.1 kJ mol^{-1} less stable, was (iii) with the positions *trans* to water and nitrate groups occupied by respectively a bromine and iodine atoms (Ag···Br = 3.379 Å and Ag···I = 3.127 Å). The last two structures, (ii) and (iv), are noticeably higher in energy (ΔE = 20.4 and 22.5 kJ mol^{-1} respectively) and have both the position *trans* to nitrate anion occupied by bromine atom.

This small DFT energy difference between (i) and (iii) is coherent with the small difference observed on the halogen atom occupancies on positions *trans* to water molecule obtained from X-ray diffraction (0.556(5) for I and 0.444(5) for Br): as (i) is slightly more stable than (iii) then an occupation factor slightly larger (smaller) than $\frac{1}{2}$ is expected for iodine (bromine). Thus, the observed partial disorder in CP **C4** could be rationalized by these quantum chemistry calculations. As shown by the latter, this disorder arose from the fact that the position *trans* to nitrate anion is strongly preferably occupied by an iodine atom, whereas the position *trans* to the water molecule can be more or less equally well occupied by iodine or bromine atoms.

As in the preceding CPs derived from the brominated bipyridine **L2**, the Ag–bipyridine chain arrangement and their linkages do not allow enough open space to lead to MOFs.

Ag(I) CPs/MOFs from chiral racemic and enantiomerically pure bipyridine L5

In order to produce homochiral MOFs based on atropisomerically chiral 4,4′-bipyridines, ligand **L5** was designed according to the following considerations. As known and shown in the preceding structures, the neutral ditopic 4,4′-bipyridine scaffold allow the 1D propagation of coordination networks. The presence of halogen atoms further connects these chains through halogen bonds. These halogens, especially bromine and iodine atoms also block the rotation around the pyridine–pyridine bond and thus stabilize the chirality of such ligands. Substituents at 5,5′-positions may contribute to enhance the asymmetric environment of the cavity and to modulate the MOF pore size.

Ligand **L5** represents a new family of heteroaromatic linkers, but readily available.[15b] Furthermore, bipyridine **L5** bearing *p*-methoxyphenyl groups can be efficiently enantioseparated by chiral HPLC on a 200 mg scale.[16a] Therefore, racemic and enantiomerically pure forms of **L5** (*rac*-**L5** and (*M*)-**L5**) were employed to build up CPs and/or MOFs. The formation of CPs with $AgNO_3$ was investigated with both the *rac*-**L5** and (*M*)-**L5**. Rewardingly, both provided suitable crystals for XRD analysis (see Table S3, ESI†).

In the centrosymmetric $[Ag(rac\text{-}\mathbf{L5})_2(NO_3)]_n$ structure **C5a**, linear bipyridine···silver chains are again found (Ag···N = 2.225 Å, 2.248 Å) as expected (Fig. 8). However, the coordination about the metal center is also ensured by three oxygen atoms of two nitrate anions (Ag···O = 2.632 Å, 2.823 Å and 2.785 Å) and a nitrogen atom of a mono-coordinated bipyridine molecule (Ag···N = 2.551 Å). Interestingly, enantiomeric bipyridines alternate along the bipyridine···silver chain, with each silver atom acting as a symmetry point. Such arrangement would have created useful voids between these chains, but an extra bipyridine fills it, while coordinating the silver atom. Therefore,

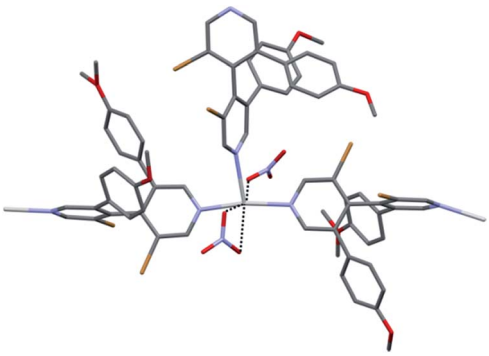

Fig. 8 Coordination around silver atom in $[Ag(rac\text{-}\mathbf{L5})_2(NO_3)]_n$ CP **C5a**. Hydrogen atoms were omitted for clarity. The almost linear bipyridine···silver chain is displayed horizontally.

a dense structure is achieved by this organization. Unfortunately, evaluation by theoretical calculation of other potential coordination modes was unsuccessful due to the large size of the system under investigation.[34]

In the non-centrosymmetric $\{[Ag_2((M)\text{-}\mathbf{L5})_2(NO_3)_2]_2\cdot iPrOH\}_n$ structure **C5b**, two crystallographically independent ligand units form two infinite bipyridine···silver linear chains. The two Ag(I) ions are further coordinated by two nitrate oxygen atoms each (Ag···O = 2.600 Å, 2.621 Å and 2.555 Å, 3.068 Å) and one can also observe a proximity of the methoxy oxygen atoms (Ag···OMe = 3.275 Å, 3.493 Å) (Fig. 9).

Both crystallographically independent bipyridine···silver chains are parallel to [100] direction. They form planes parallel to (001) where the chains interact through the silver···nitrate···silver bonds reported above. No clear π–π stacking between the methoxyphenyl rings can be evidenced, the centroid–centroid inter-ring smallest distance being 5.008 Å and the angle between the rings planes being 52.9°. Therefore, the cohesion between these planes surprisingly seems to only involve silver···OMe contacts and presumably steric fit between adjacent planes.

In sharp contrast to the dense structure obtained with *rac*-**L5**, the **C5b** structure gained from enantiomerically pure bipyridine (*M*)-**L5** displays channels parallel to the [100] crystallographic direction having free aperture of 4.0 Å× 5.2 Å and in which solvent molecules are located. These solvent accessible voids amount to 21.4% of the unit cell volume (evaluated with a probe radius of 1.2 Å, using the Platon software[35]) (Fig. 10).

The **C5b** structure thus represents a homochiral MOF, remarkable *per se* but also for the large size of its pores. On this basis, in order to get an insight into recognition capability and bioactivity of the homochiral network based on **L5**, its thermostability, enantioseparation capability and *in vitro* cytotoxicity were examined.

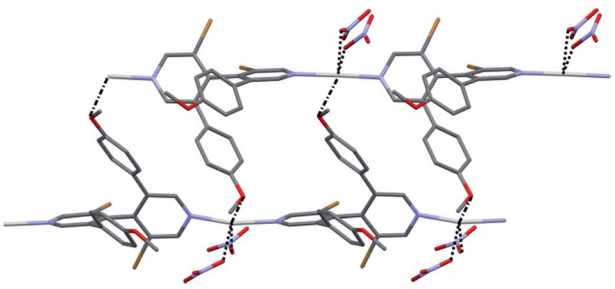

Fig. 9 Coordination around silver atom in $[Ag((M)\text{-}\mathbf{L5})NO_3]_2\cdot iPrOH$ MOF **C5b**. Hydrogen and disordered silver atoms and solvent molecules were omitted for clarity. The two crystallographic independent almost linear bipyridine···silver chain are displayed horizontally. Nitrate···silver interactions are shown as dashed lines, OMe···silver as dotted-dashed lines.

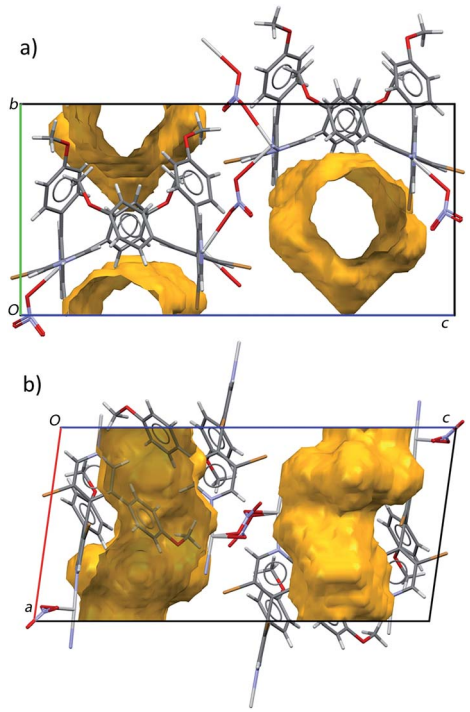

Fig. 10 Non-centrosymmetric crystal structure of $\{[Ag_2((M)\text{-}\mathbf{L5})_2\text{-}(NO_3)_2]_2\cdot iPrOH\}_n$ MOF **C5b** displaying the channels parallel to [100] crystallographic direction. Contact surface with a probe radius of 1.2 Å are shown in gold. Isopropanol solvent molecules located inside these channels are omitted for clarity. (a) View along [100]. (b) View along [010]*.

Preliminary applications of the so-obtained Ag(I) MOF

Stability. Before any application, we investigated the stability towards heat of this new MOF. For comparison purposes, we also looked at the stability of its analogue **C5a** produced from *rac*-**L5**. Both **C5a** and **C5b** were thus submitted to thermogravimetric analysis (TGA) from 20 to 800 °C in flowing helium at 3 °C min^{-1} (Fig. S5, ESI†).

Due to its more compact structure, **C5a** was expected to be more stable than **C5b**. Furthermore, the latter contains relatively weak silver···OMe interactions between bipyridine···silver planes, suggesting again a lower stability. Rewardingly, both silver CPs remain stable up to about 200 °C. Nevertheless, a slight but sole difference was observed for **C5b**, for which a weight loss of about 10% was observed around 130 °C. As shown by mass spectrometry (MS) analysis coupled with TGA, this weight loss corresponds to the release of isopropanol, embedded in the **C5b** framework (see X-ray structure in ESI†) Accordingly, **C5a** does not show any signal attributable to isopropanol release. Further heating of the samples leads to the slow collapse of the framework structures owing to decomposition of the 4,4′-bipyridine ligands.

Enantioselective adsorption of small racemic molecules on $Ag((P)\text{-}\mathbf{L5})NO_3$

Enantioselective adsorption of racemic organic compounds on chiral MOFs has been a continuing challenge due to the ever-increasing importance of enantiomerically pure compounds to fine chemical and pharmaceutical industries.[36] Indeed, chiral MOFs could become an interesting alternative to the chiral

supports currently used to separate enantiomers by chiral chromatography.

Thus, we briefly examined the possibility to discriminate enantiomers on a sample of Ag((*P*)-**L5**)NO_3 MOF whose crystal structure was checked to be enantiomorphic with **C5b**. Taking into account that the dimensions of the racemates could have a deep impact on the encapsulation process, three racemates, namely *rac*-benzoin, *rac-trans*-stilbene oxide and *rac*-styrene oxide were selected for comparison, having CPK volume values of 229.0 $Å^3$, 221.3 $Å^3$ and 137.3 $Å^3$, respectively (Fig. S6a, ESI†). As mentioned above, the permanent porosity of Ag((*P*)-**L5**)NO_3 is characterized by small dimension, so we speculate that only the styrene oxide could be able to enter through the chiral network, while this MOF should exert a sort of molecular sieve-like behaviour toward the two larger racemates. On the other hand, so far enantioseparation experiments as well as computational studies have confirmed that, despite the chirality of the MOF framework obviously assists the separation mechanism, the more dominant factor is the perfect match between the guest analyte and the framework size and shape.[37]

For each racemate, the crystals of Ag((*P*)-**L5**)NO_3 were used as synthesized. The crystals were immersed in 500 μL of a 0.1 M ethyl ether solution of the racemic compound (styrene oxide/MOF 3 : 1) with no stirring or shaking for 5 days at 25 °C. After this time, crystals were filtered and washed with ethyl ether (2 × 1 mL) to remove the residual chiral compound from the surface of the crystals. The filtrate and extracts were then analyzed by chiral HPLC to determine ee values. As expected, only the styrene oxide was enantioselectively adsorbed under these conditions. From the available data (Fig. S6b, ESI†), a 16% ee was detected by HPLC on chiral stationary phase. This promising result prove the encapsulation of the (*S*)-enantiomer.

***In vitro* cytotoxicity of Ag(L5) complexes.** The unique adsorbent properties of MOFs have been extensively developed and applied to gas storage and separation, and more recently it led to the rapid development of new applications in areas related to biomedicine.[20b] In this field, the most widely used metals for preparing bioactive MOFs are Ca, Mg, Zn, Fe, Ti or Zn, which exhibit acceptable toxicity,[37] while the study of Ag–MOFs as antibacterial agents is still in its infancy.[20]

In this context, we evaluated the toxic profile of complexes **C5a** and **C5b** in epidermis resident cells in order to assess the safety and the potential for dermal drug delivery of these formulations.

We investigated *in vitro* the effect of silver complexes Ag(*rac*-**L5**)$_2NO_3$ and Ag((*M*)-**L5**)NO_3 in a cell line derived from adult human skin (HaCaT) that exhibits normal differentiation capacity and a DNA fingerprint pattern unaffected by long-term cultivation. Both the racemic and the homochiral Ag-based complexes were stable with regard to water and this observation opened the possibility to investigate their biocompatibility. The effect of the enantiopure linker (*M*)-**L5** was also measured in order to exclude an intrinsic activity due to the linker itself.

Cytotoxicity was determined with MTT assay after different time points (24–48–72 hours). At each time point, the effect of all tested compounds looked to be concentration dependent. A threshold of 75% cell viability was arbitrarily assigned to discriminate the severity of the cytotoxic effect observed. As shown in Fig. 11, while the linker (*M*)-**L5** and Ag(*rac*-**L5**)$_2NO_3$ exhibited a severe reduction of cell viability (>75%) at concentration higher than 3 μM, the homochiral complex Ag((*M*)-**L5**)NO_3 exhibited a relevant cytotoxic effect only at the highest concentration tested (30 μM). These results revealed the safer profile associated with the homochiral and porous network of Ag((*M*)-**L5**)NO_3 MOF, opening new and promising developments towards further biomedical applications.

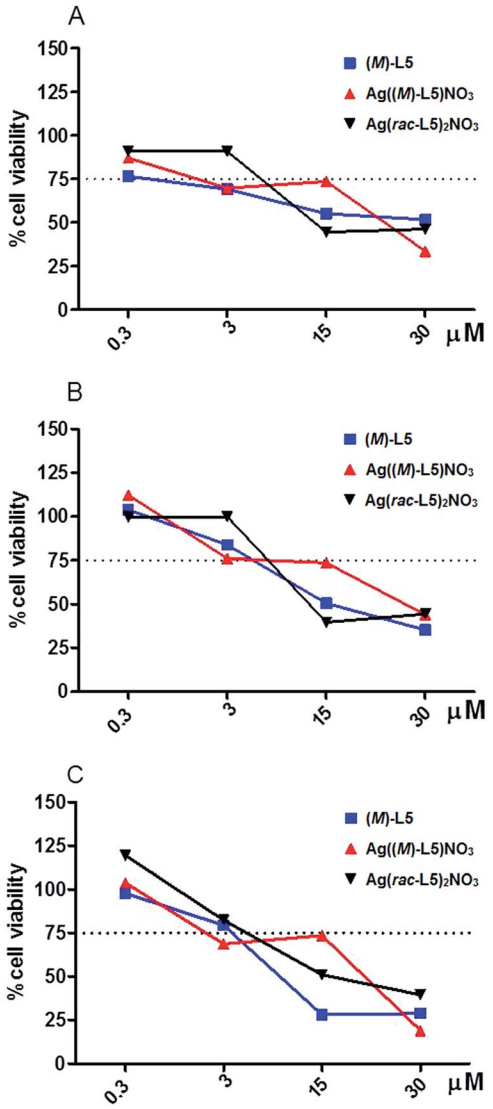

Fig. 11 *In vitro* cytotoxicity of Ag-based complexes: (A) (24 h), (B) (48 h), (C) (72 h).

Conclusions

Through this paper, we showed that 3,3′,5,5′-tetrasubstituted 4,4′-bipyridines represent valuable ligands for the design of silver coordination polymers (Ag-CPs). Eleven new Ag-CPs and MOFs have been obtained including a chiral one. Both achiral and chiral ligands have been studied highlighting the benefit of the peripheral substituents around the 4,4′-bipyridine skeleton.

Halogen atoms can participate in the coordination of the metal center, whereas bulkier aromatic substituents can lead to a porous network. In this regard, the first homochiral MOF based on an atropisomeric 4,4′-bipyridine ligand has been described and its recognition capability has been briefly examined by means of enantioselective adsorption. Discrimination was observed for styrene oxide, and further work in this area is underway in our group.

Moreover, the cytotoxicity on HaCaT cells was evaluated. The first results obtained show that this new type of homochiral complexes is toxicologically acceptable for further investigations related to biological applications. Further works on the design and synthesis of homochiral MOFs based on atropisomeric ditopic 4,4′-bipyridine linkers are currently underway in our group.

Acknowledgements

CNRS, Université de Lorraine and Université de Strasbourg are acknowledged for financial support. The Service Commun de Diffraction X of Université de Lorraine is thanked for providing access to crystallographic facilities. This work was granted access to the HPC resources of CINES/CEA CCRT/IDRIS under the allocation x2016087449 made by GENCI. Viviana Marolda is thanked for her technical assistance with the *in vitro* assays.

Notes and references

1 (*a*) D. J. Tranchemontagne, J. L. Mendoza-Cortés, M. O'Keeffe and O. M. Yaghi, *Chem. Soc. Rev.*, 2009, **38**, 1257; (*b*) S. R. Batten, N. R. Champness, X.-M. Chen, J. Garcia-Martinez, S. Kitagawa, L. Öhrström, M. O'Keeffe, M. P. Suh and J. Reedijk, *Pure Appl. Chem.*, 2013, **85**, 1715.

2 B. Li, H.-M. Wen, Y. Cui, W. Zhou, G. Qian and B. Chen, *Adv. Mater.*, 2016, **28**, 8819.

3 X. Lin, N. R. Champness and M. Schroder, *Top. Curr. Chem.*, 2010, **293**, 35.

4 R. Zou, A. I. Abdel-Fattah, H. Xu, Y. Zhao and D. D. Hickmott, *CrystEngComm*, 2010, **12**, 1337.

5 P. Garcia-Garcia, M. Muller and A. Corma, *Chem. Sci.*, 2014, **5**, 2979.

6 (*a*) I. Nath, J. Chakraborty and F. Verpoort, *Chem. Soc. Rev.*, 2016, **45**, 4127; (*b*) D. Liu, K. Lu, C. Poon and W. Lin, *Inorg. Chem.*, 2014, **53**, 1916.

7 M. Yoon, R. Srirambalaji and K. Kim, *Chem. Rev.*, 2012, **112**, 1196.

8 (*a*) P. Peluso, V. Mamane and S. Cossu, *J. Chromatogr. A*, 2014, **1363**, 11; (*b*) T. Duerinck and J. F. M. Denayer, *Chem. Eng. Sci.*, 2015, **124**, 179.

9 Selected recent examples: (*a*) D. De, T. K. Pal and P. K. Bharadwaj, *Inorg. Chem.*, 2016, **55**, 6842; (*b*) C. Kutzscher, G. Nickerl, I. Senkovska, V. Bon and S. Kaskel, *Chem. Mater.*, 2016, **28**, 2573; (*c*) N. Ye, J. Ma, J. An, J. Li, Z. Cai and H. Zong, *RSC Adv.*, 2016, **6**, 41587; (*d*) M. Zhang, X. Chen, J. Zhang, J. Kong and L. Yuan, *Chirality*, 2016, **28**, 340; (*e*) J. Bonnefoy, A. Legrand, E. A. Quadrelli, J. Canivet and D. Farrusseng, *J. Am. Chem. Soc.*, 2015, **137**, 9409.

10 (*a*) C. Zhu, Q. Xia, X. Chen, Y. Liu, X. Du and Y. Cui, *ACS Catal.*, 2016, **6**, 7590; (*b*) Q. Xia, Y. Liu, L. Zijian, W. Gong and Y. Cui, *Chem. Commun.*, 2016, **52**, 13167; (*c*) A. Bhunia, S. Dey, J. M. Moreno, U. Diaz, P. Concepcion, K. Van Hecke, C. Janiak and P. Van Der Voort, *Chem. Commun.*, 2016, **52**, 1401; (*d*) W. Xi, Y. Liu, Q. Xia, Z. Li and Y. Cui, *Chem.–Eur. J.*, 2015, **21**, 12581.

11 Selected recent examples for biphenyls: (*a*) N. L. Strutt, D. Fairen-Jimenez, J. Iehl, M. B. Lalonde, R. Q. Snurr, O. K. Farha, J. T. Hupp and J. F. Stoddart, *J. Am. Chem. Soc.*, 2012, **134**, 17436; (*b*) Y. Peng, T. Gong, K. Zhang, X. Lin, Y. Liu, J. Jiang and Y. Cui, *Nat. Commun.*, 2014, **5**, 1; for binaphtyls: (*c*) K. Tanaka, T. Muraoka, Y. Otubo, H. Takahashi and A. Ohnishi, *RSC Adv.*, 2016, **6**, 21293; (*d*) T. Sawano, N. C. Thacker, Z. Lin, A. R. McIsaac and W. Lin, *J. Am. Chem. Soc.*, 2015, **137**, 12241; (*e*) M. Lee, S. M. Shin, N. Jeong and P. K. Thallapally, *Dalton Trans.*, 2015, **44**, 9349.

12 (*a*) K. Birasha, M. Sarkar and L. Rajput, *Chem. Commun.*, 2006, 4169; (*b*) E. Aubert, A. Doudouh, P. Peluso and V. Mamane, *Acta Crystallogr.*, 2016, **E72**, 1654.

13 L. Sbircea, N. D. Sharma, W. Clegg, R. W. Harrington, P. N. Horton, M. B. Hursthouse, D. C. Apperley, D. R. Boyd and S. L. James, *Chem. Commun.*, 2008, 5538.

14 A. Rang, M. Engeser, N. M. Maier, M. Nieger, W. Lindner and C. A. Schalley, *Chem.–Eur. J.*, 2008, **14**, 3855.

15 (*a*) M. Abboud, V. Mamane, E. Aubert, C. Lecomte and Y. Fort, *J. Org. Chem.*, 2010, **75**, 3224; (*b*) V. Mamane, E. Aubert, P. Peluso and S. Cossu, *J. Org. Chem.*, 2012, **77**, 2579; (*c*) V. Mamane, E. Aubert, P. Peluso and S. Cossu, *J. Org. Chem.*, 2013, **78**, 7683; (*d*) V. Mamane, P. Peluso, E. Aubert, S. Cossu and P. Pale, *J. Org. Chem.*, 2016, **81**, 8576.

16 (*a*) P. Peluso, V. Mamane, E. Aubert and S. Cossu, *J. Chromatogr. A*, 2012, **1251**, 91; (*b*) P. Peluso, V. Mamane, E. Aubert and S. Cossu, *J. Sep. Sci.*, 2013, **36**, 2993; (*c*) P. Peluso, V. Mamane, E. Aubert and S. Cossu, *J. Chromatogr. A*, 2014, **1345**, 182; (*d*) P. Peluso, V. Mamane, E. Aubert and S. Cossu, *J. Sep. Sci.*, 2014, **37**, 2481; (*e*) P. Peluso, V. Mamane, E. Aubert, A. Dessi, R. Dallocchio, A. Dore, P. Pale and S. Cossu, *J. Chromatogr. A*, 2016, **1467**, 228.

17 A. N. Khlobystov, A. J. Blake, N. R. Champness, D. A. Lemenovskii, A. G. Majouga, N. V. Zyk and M. Schröder, *Coord. Chem. Rev.*, 2001, **222**, 155.

18 H. Schmidbaur and A. Schier, *Angew. Chem., Int. Ed.*, 2015, **54**, 746.

19 J.-H. Chen, Y.-M. Liu, J.-X. Zhang, Y.-Y. Zhu, M.-S. Tang, S. W. Ng and G. Yang, *CrystEngComm*, 2014, **16**, 4987.

20 (*a*) M. Berchel, T. Le Gall, C. Denis, S. Le Hir, F. Quentel, C. Elléouet, T. Montier, J.-M. Rueff, J.-Y. Salaün, J.-P. Haelters, G. B. Hix, P. Lehn and P.-A. Jaffrès, *New J. Chem.*, 2011, **35**, 1000; (*b*) P. Horcajada, R. Gref, T. Baati, P. K. Allan, G. Maurin, P. Couvreur, G. Férey, R. E. Morris and C. Serre, *Chem. Rev.*, 2012, **112**, 1232.

21 (*a*) K. Kawahara, K. Tsuruda, M. Morishita and M. Uchida, *Dent. Mater.*, 2000, **16**, 452; (*b*) Ç. Çınar, T. Ulusu, B. Özçelik, N. Karamüftüoğlu and H. Yücel, *J. Biomed. Mater. Res., Part B*, 2009, **90B**, 592; (*c*) B. Dong, S. Belkhair, M. Zaarour, L. Fisher, J. Verran, L. Tosheva, R. Retoux, J.-P. Gilsona and S. Mintova, *Nanoscale*, 2014, **6**, 10859.

22 R. C. Clark and J. S. Reid, *Acta Crystallogr., Sect. A: Found. Crystallogr.*, 1995, **51**, 887.

23 L. J. Farrugia, *J. Appl. Crystallogr.*, 2012, **45**, 849.

24 (*a*) A. Altomare, G. Cascarano, C. Giacovazzo, A. Guagliardi, M. C. Burla, G. Polidori and M. Camalli, *J. Appl. Crystallogr.*, 1994, **27**, 435; (*b*) G. M. Sheldrick, *SHELXL-97, Program for the Refinement of Crystal Structures*, University of Göttingen, Germany, 1997.

25 C. F. Macrae, P. R. Edgington, P. McCabe, E. Pidcock, G. P. Shields, R. Taylor, M. Towler and J. van de Streek, *J. Appl. Crystallogr.*, 2006, **39**, 453.

26 M. J. Frisch, G. W. Trucks, H. B. Schlegel, G. E. Scuseria, M. A. Robb, J. R. Cheeseman, G. Scalmani, V. Barone, B. Mennucci, G. A. Petersson, H. Nakatsuji, M. Caricato, X. Li, H. P. Hratchian, A. F. Izmaylov, J. Bloino, G. Zheng, J. L. Sonnenberg, M. Hada, M. Ehara, K. Toyota, R. Fukuda, J. Hasegawa, M. Ishida, T. Nakajima, Y. Honda, O. Kitao, H. Nakai, T. Vreven, J. A. Montgomery Jr, J. E. Peralta, F. Ogliaro, M. Bearpark, J. J. Heyd, E. Brothers, K. N. Kudin, V. N. Staroverov, T. Keith, R. Kobayashi, J. Normand, K. Raghavachari, A. Rendell, J. C. Burant, S. S. Iyengar, J. Tomasi, M. Cossi, N. Rega, J. M. Millam, M. Klene, J. E. Knox, J. B. Cross, V. Bakken, C. Adamo, J. Jaramillo, R. Gomperts, R. E. Stratmann, O. Yazyev, A. J. Austin, R. Cammi, C. Pomelli, J. W. Ochterski, R. L. Martin, K. Morokuma, V. G. Zakrzewski, G. A. Voth, P. Salvador, J. J. Dannenberg, S. Dapprich, A. D. Daniels, O. Farkas, J. B. Foresman, J. V. Ortiz, J. Cioslowski, and D. J. Fox, Gaussian 09, Revision B.01, Inc., Wallingford CT, 2010.

27 AIMAll, Todd A. Keith, TK Gristmill Software, Overland Park KS, USA, 2015 (http://aim.tkgristmill.com).

28 S. J. Clark, M. D. Segall, C. J. Pickard, P. J. Hasnip, M. J. Probert, K. Refson and M. C. Payne, *Z. Kristallogr.*, 2005, **220**, 567.

29 J. P. Perdew, K. Burke and M. Ernzerhof, *Phys. Rev. Lett.*, 1996, **77**, 3865.

30 S. J. Grimme, *Comput. Chem.*, 2006, **27**, 1787.

31 A. Bondi, *J. Phys. Chem.*, 1964, **68**, 441.

32 (*a*) T. Sakurai, M. Sundaralingam and G. A. Jeffrey, *Acta Crystallogr.*, 1963, **16**, 354; (*b*) N. Ramasubbu, R. Parthasarathy and P. Murray-Rust, *J. Am. Chem. Soc.*, 1986, **108**, 4308; (*c*) G. R. Desiraju and R. Pathasarathy, *J. Am. Chem. Soc.*, 1989, **111**, 8725; (*d*) E. Aubert, S. Lebègue, M. Marsman, T. T. T. Bui, C. Jelsch, S. Dahaoui, E. Espinosa and J. G. Ángyán, *J. Phys. Chem. A*, 2011, **115**, 14484.

33 M. E. Brezgunova, E. Aubert, S. Dahaoui, P. Fertey, S. Lebègue, C. Jelsch, J. G. Ángyán and E. Espinosa, *Cryst. Growth Des.*, 2012, **12**, 5373.

34 Periodic DFT computations have been attempted on modifications of **C5a** presenting different alternation of bipyridine enantiomers along the bipyridine···silver chains, but without success due to the large size of the system. Such calculations are presently beyond the capacity of our available computation resources.

35 A. L. Spek, *Acta Crystallogr.*, 2009, **D65**, 148.

36 S. Keskin and S. Kizilel, *Ind. Eng. Chem. Res.*, 2011, **50**, 1799.

37 (*a*) Y.-M. Song, T. Zhou, X.-S. Wang, X.-N. Li and R.-G. Xiong, *Cryst. Growth Des.*, 2006, **6**, 14; (*b*) S.-Y. Zhang, L. Wojtas and M. J. Zaworotko, *J. Am. Chem. Soc.*, 2015, **137**, 12045; (*c*) X. Bao, L. J. Broadbelt and R. Q. Snurr, *Mol. Simul.*, 2009, **35**, 50; (*d*) P. Z. Moghadam and T. Düren, *J. Phys. Chem. C*, 2012, **116**, 20874; (*e*) X. Kuang, Y. Ma, H. Su, J. Zhang, Y.-B. Dong and B. Tang, *Anal. Chem.*, 2014, **86**, 1277; (*f*) Z. Qiao, A. Torres-Knoop, D. Dubbeldam, D. Fairen-Jimenez, J. Zhou and R. Q. Snurr, *AIChE J.*, 2014, **60**, 2324.